Journal of Environmental Science International
33(9); 633~643; September 2024

pISSN: 1225-4517 eISSN: 2287-3503
https://doi.org/10.5322/JESI.2024.33.9.633

ORIGINAL ARTICLE

Eco-Friendly Photocatalytic Transformation of Greenhouse Gas CO_2 into Precious CH_4 Fuel via Cu-Deposited Black TiO_2 under Simulated Sunlight Irradiation

Dong Jin Kim, Hyun-Cheol Lee[1)], Seung-Ho Shin[1)], Wan-Kuen Jo[*]

School of Architecture, Civil, Environmental and Energy Engineering, Kyungpook National University, Daegu 41566, Korea

[1)]JIGU Environment and Consulting Inc., Pohang, Gyeongsangbuk-do 37596, Korea

Abstract

Hereunder, the eco-friendly photocatalytic CO_2 transformation capability of Cu-deposited black TiO_2 (Cu/BTiO$_2$) was evaluated to investigate if this photocatalyst proceeds the thermodynamically- and kinetically-satisfactory CO_2 transformation into CH_4. The clustered Cu-deposited BTiO$_2$ (Cu/BTiO$_2$) and Cu/BTiO$_2$ architectures revealed noticeable photocatalytic CO_2 transformation abilities, whereas the pristine TiO_2 and BTiO$_2$ catalysts displayed no significant photocatalytic CO_2 transformation abilities. Especially, the photocatalytic CO_2 transformation rates of a representative Cu/BTiO$_2$ architecture were 104, 209, 272, 322, and 361 ㎛ol/g at the irradiation times of 2, 4, 6, 8, and 10 h, respectively, while the photocatalytic CO_2 transformation rates of Cu/BTiO$_2$ were 61, 139, 217, 270, and 309 ㎛ol/g at the same irradiation times, respectively. The promoted photocatalytic CO_2 transformation ability of the Cu/BTiO$_2$ architecture was assigned to the excellent electron–hole separation tendency, which was verified by the photoluminescence analysis. The composition ratio of Cu incorporated into BTiO$_2$ in the Cu/BTiO$_2$ architectures was crucial in CH_4 generation. In addition, the Cu/BTiO$_2$ architecture displayed eminent photodurability, which was verified by the consecutive experiment cycle, and the mechanistic process for CO_2 transformation into CH_4 via the Cu/BTiO$_2$ architecture was established. The electronic framework of the Cu/BTiO$_2$ architecture was established on the basis of its band gap and valence band value. Conclusively, the Cu/BTiO$_2$ architecture is an outstanding tool for thermodynamically- and kinetically-satisfactory photocatalytic CO_2 transformation into CH_4 that application under simulated sunlight irradiation.

Key words : Clustered Cu, Thermodynamically-satisfactory, Kinetically-satisfactory, Experiment cycle, Photodurability

1. Introduction

With the ever-increasing combustion of hydrocarbon-containing fuels, the greenhouse gas concentration in the atmosphere is gradually elevating, which leads to substantial problems about the detrimental impacts on the climate and energy shortage crisis (Lewis, 2019; Liao et al., 2019; Dong et al., 2020; Li et al., 2021; Zhang et al., 2021; Tang et al., 2023; Majumdar et al., 2024). This crucial environmental issue prompts the urgent development of the effective techniques for the mitigation of CO_2 emission into the atmosphere. Typically, much efforts have been given to explore the thermocatalytic techniques for CO_2 transformation into precious

Received 18 July, 2024; **Revised** 28 August, 2024;
Accepted 30 August, 2024
***Corresponding author** : Wan-Kuen Jo, School of Architecture, Civil, Environmental and Energy Engineering, Kyungpook National University, Daegu 41566, South Korea
Phone : +82-53-950-6584
E-mail : wkjo@knu.ac.kr.

chemicals (Bermejo-López et al., 2019; Chen et al., 2020; Xu et al., 2020). However, in the conventional thermocatalytic CO_2 transformation method, hydrogen gas is employed as reducing material to produce hydrogen atoms for the formation of reactive electrons, which causes explosive risks and high costs (Bermejo-López et al., 2019; Chen et al., 2020; Xu et al., 2020). Fortunately, artificially-mimicked photosynthesis using the solar light-activated photocatalytic process has been recently suggested as an optimistic approach to address the energy shortage as well as atmospheric CO_2 level mitigation by transforming CO_2 into precious fuels such as CH_4 and other hydrocarbons (Chen et al., 2019; Choi et al., 2019; Li et al., 2019; Pan et al., 2019; Xie et al., 2019; Zhang et al., 2021; Cheng et al., 2024). In addition, CO_2 is potentially be converted into valuable chemicals that are utilized in various industrial processes (Pan et al., 2019; Xie et al., 2019; Zhang et al., 2021). Semiconductor–based photocatalysts have been most widely utilized for CO_2 transformation to precious materials due to their prominent photodurabilty and appropriate electron structures for CO_2 reduction reaction (Jiang et al., 2018; Wu et al., 2019; Guo et al., 2020; Xiong et al., 2020; Zeng et al., 2021; Zhao et al., 2021). In spite of tremendous efforts, the photocatalytic CO_2 transformation technique is yet challenging due to its thermodynamically and kinetically unfavorable reaction pathways (Li et al., 2021; Zhang et al., 2021). Thus, high-performance photocatalytic techniques with thermodynamically and kinetically favorable CO_2 transformation pathway are necessary to overcome the aforementioned problems.

To accomplish the thermodynamically-approving CO_2 transformation pathway into a precious fuel CH_4, the conduction band of a photocatalyst must be negative than the CO_2/CH_4 reduction potential of −0.24 eV (Fang and Wang, 2018; Zhou et al., 2018; Wang et al., 2021). Among the popularly employed photocatalysts, TiO_2 has received tremendous interests in its photocatalytic application to CO_2 transformation because of its prominent photostability and higher conduction band value (−0.61 eV) than the CO_2/CH_4 reduction potential (Wang et al., 2019a; Wang et al., 2019b; Xiong et al., 2020; Zhang et al., 2021). Nonetheless, pristine TiO_2 shows an unacceptable photocatalytic capability and low quantum yields under visible-light irradiation due to its fast carrier recombination rate and wide bandgap, respectively, significantly inhibiting its actual utilization to the photocatalytic CO_2 transformation under visible-light irradiation (Shi et al., 2019; Zhang et al., 2021). This limitation may be overcome by modifying TiO_2 into black TiO_2, which can increase optical efficiencies of TiO_2 due to the disordered structure, transformed electron properties, and a range of defect groups (Ullattil et al., 2018; Rajaraman et al., 2020).

To achieve kinetically-satisfactory CO_2 transformation pathway into CH_4, the carrier separation efficiency of the photocatalyst should be considered (Fang and Wang, 2018; Zhou et al., 2018; Wang et al., 2021). The surface alteration of photocatalysts by depositing a pertinent metal cocatalyst can promote its separation efficiency of carriers due to the high carrier transportability at interfaces of photocatalyst–cocatalyst (Shen et al., 2019; Yi et al., 2019; Ishii et al., 2020). The non-precious metal copper (Cu) can be utilized as a potential cocatalyst because of its prominent charge acceptance nature, which promotes the carrier separation rates (Chen et al., 2018; Maldonado et al., 2018; Liu et al., 2019; Ge et al., 2020). Markedly, compared to conventional aggregated metal cocatalysts, metal cocatalysts show greater probability for providing more reactive spots

and cost moderation, prompting their utilization in the advancement of potential metal-deposited photocatalysts (Wei et al., 2019; Gao et al., 2020; Li et al., 2020).

In this study, the photocatalytic CO_2 transformation capability of Cu-deposited black TiO_2 (Cu/BTiO_2) was evaluated to examine whether this photocatalyst follows the thermodynamically-and kinetically-satisfactory CO_2 transformation into CH_4. For comparison, selected reference samples (i.e., pristine TiO_2, black TiO_2 (BTiO_2), and conventional aggregated Cu-deposited BTiO_2 (Cu/BTiO_2)) were evaluated for the photocatalytic CO_2 transformation into CH_4. Further, probable mechanistic insight into the photocatalytic CO_2 transformation into CH_4 via Cu/BTiO_2 was investigated, and the photostability of this photocatalyst was assessed through a recycling test.

2. Methods

2.1. Photocatalyst fabrication

The BTiO_2 sample was fabricated by reducing pristine TiO_2 using a temperature-programmed electric furnace under H_2 (30 mL/min)/Ar (470 mL/min) gas flow conditions. In brief, pristine TiO_2 powder (4.0 g) was dispersed in an alumina boat and placed at the central site of a quartz tube in the electric furnace. The reduction process was carried out in the furnace heated to 400°C and kept for 5 h. The reducing compounds were cleaned with deionized water, filtered, and dried at 85°C for 10 h to obtain the BTiO_2 photocatalyst.

The Cu/BTiO_2 samples was fabricated by photodepositing Cu onto the BTiO_2 powder. For this procedure, BTiO_2 powder (0.1 g) was suspended into deionized water (0.1 L) to prepare solution A. In addition, $Cu(NO_3)_2{\cdot}3H_2O$ (0.95 g) was dispersed to deionized water (0.25 L) to prepare solution B. Subsequently, solution B (1, 1.2, 1.4, 1.6, 1,8, or 2 mL) was slowly added to solution A, after which this solution was stirred for 0.5 h to obtain a homogeneous solution. The mixture was then transferred to a Pyrex reactor equipped with a quartz window. After closing all openings of the reactor, the solution was purged using pure CO_2 for 0.5 h and irradiated by a 350-W Xe for 4 h. Finally, the suspension was vacuum-treated and washed using ethanol, and the resultant precipitate was dried and ground to obtain Cu/BTiO_2 sample. The Cu/BTiO_2 samples prepared using $Cu(NO_3)_2{\cdot}3H_2O$ solution amounts of 1, 1.2, 1.4, 1.6, 1.8, and 2 mL were denoted as Cu/BTiO_2-1, Cu/BTiO_2-1.2, Cu/BTiO_2-1.4, Cu/BTiO_2-1.6, Cu/BTiO_2-1.8, and Cu/BTiO_2-2, respectively. Furthermore, the Cu/BTiO_2 sample was fabricated by following the above procedure; in this case, the mixed solution in the reactor was purged using Ar instead of CO_2 gas.

2.2. Photocatalyst characterization

The fabricated materials were surveyed by X-ray diffraction (XRD) spectroscopy, transmission electron microscopy(TEM), high-resolution transmission electron microscopy (HRTEM), UV-visible spectrophotometry, X-ray photoelectron spectroscopy (XPS), and photoluminescence (PL) emission spectroscopy. XRD patterns were recorded for 2θ = 10°-80° using a Rigaku D/max-2500 diffractometer (Tokyo, Japan). The morphology of the materials was inspected using a Hitachi 7700 instrument operated at 150 kV (TEM, Hitachi, Japan). The HRTEM patterns were captured using a FEI Titan G2 ChemiSTEM Cs Probe instrument (Hillsboro, OR, USA). The UV-visible spectra were inspected using the CARY 5G Varian spectrophotometer (Cary, NC, USA). The XPS spectra were afforded using the PHI Quantera SXM instrument (Chanhassen, MN, USA. The high-resolved PL emission spectra were afforded using an Action Research Spectra Pro 2150i spectrophotometer (Princeton, NJ, USA).

2.3. Measurement of the photoelectric currents

Transient photoelectric current measurements were performed on the Ivium Technologies electrochemical workstation with triple-electrode cells. Indium tin oxide (ITO) covered by a photocatalyst was regarded as the work electrode. Ag/AgCl immersed in KCl solution and Pt film were used as the reference and counter electrodes, correspondingly. The Na_2SO_4 (0.5 M) solution was utilized as the electrolytic material. The current signals of the photocatalysts were determined via a 350-W Xe light source. The as-fabricated photocatalyst (0.02 g) was dispersed in Nafion solution (5 wt%). The solution was continuously stirred to afford a slurry-type sample, after which this slurry was placed on the ITO plate with a covered area of 1.5 cm^2. Finally, the sample-covered ITO plate was dried at 85°C for 10 h and the photocurrent generated on this ITO plate was measured using the Ivium Technologies electrochemical workstation.

2.4. Photocatalytic CO_2 transformation into CH_4

The photocatalytic capability of the as-constructed materials for CO_2 transformation into CH_4 was determined utilizing a secured stainless steel chamber (100 mL) fitted with a quartz window for light penetration. Summarily, a sample photocatalyst was dispersed in a solution of Na_2SO_4 (0.7 g), $NaHCO_3$ (0.5 g), and deionized water (0.06 L), after which the dispersion was ultrasonicated for 0.5 h. The solution was then bubbled with super-pure CO_2 for 0.5 h to saturate it with CO_2 as well as to exclude oxygen from the solution. Subsequently, all openings of the stainless steel chamber were closed, and the chamber was illuminated through the 350-W Xe light source placed at the sunlight supplier. Gas samples (500 μl) were regularly taken through the sampling port of the stainless steel chamber utilizing a gastight micro-syringe. The collected samples were qualitatively and quantitatively determined employing a gas chromatography (GC-Plus, Shimazu, Japan) installed with a thermal conductivity detection system. The quantitative investigation of the collected compounds was carried out using the calibration curve, which was established by analyses of standard gases. Furthermore, three control experiments were carried out: 1) CO_2 transformation into CH_4 in the presence of light but without the addition of a photocatalyst; 2) CO_2 transformation into CH_4 in the presence of a photocatalyst but without light; and 3) CO_2 transformation into CH_4 in the presence of light and a photocatalyst under CO_2-free conditions. The control experiments were carried out utilizing the abovementioned CO_2 transformation process.

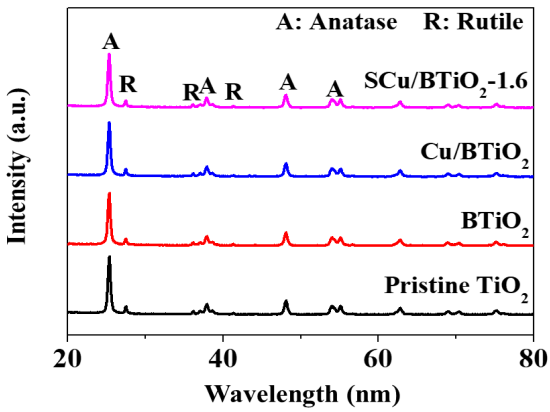

Fig. 1. X-ray diffraction patterns of pristine TiO_2, $BTiO_2$, Cu/$BTiO_2$, and Cu/$BTiO_2$-1.6.

3. Results and discussion

3.1. Material characteristics

The crystalline characteristics of pristine TiO_2, $BTiO_2$, Cu/$BTiO_2$, and Cu/$BTiO_2$-1 are presented in their XRD spectra (Fig. 1). All

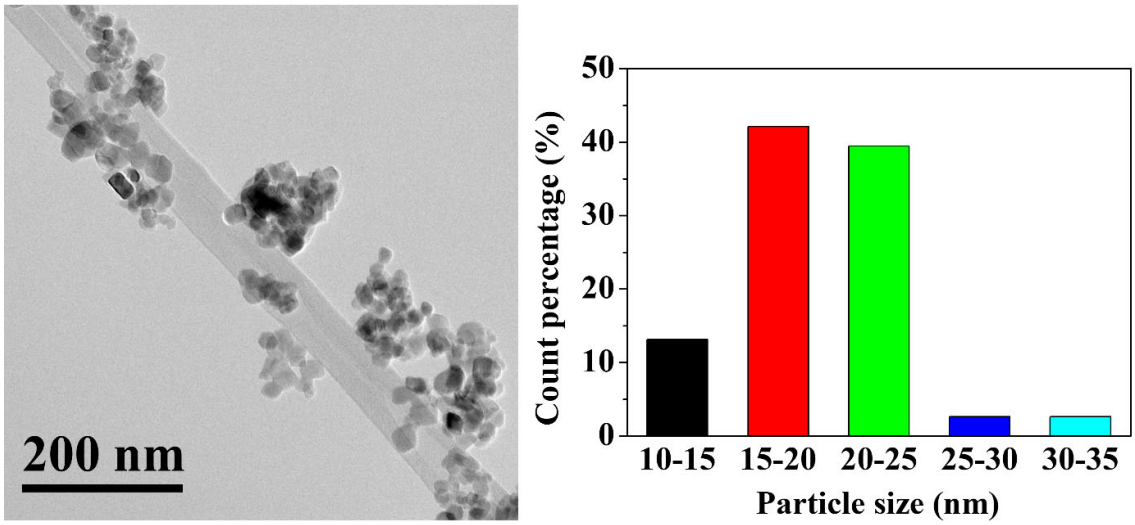

Fig. 2. Transmission electron microscopy image and size distribution of Cu/BTiO$_2$-1.6.

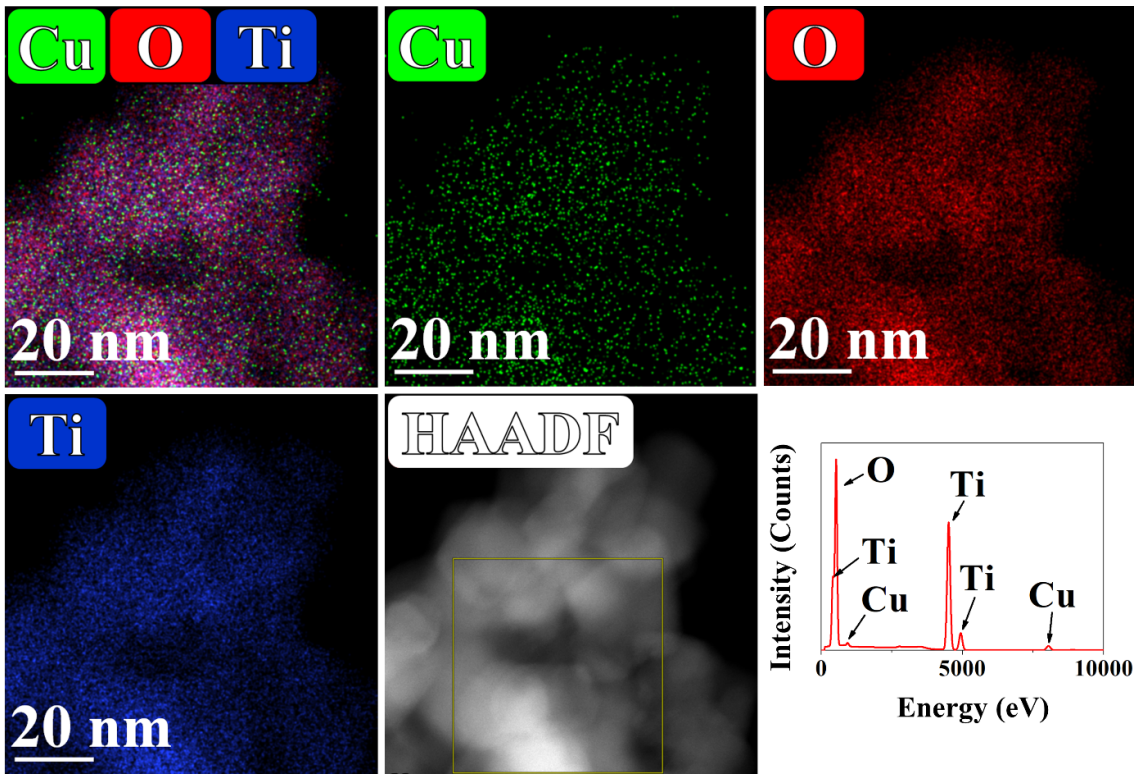

Fig. 3. Elemental mapping results and energy-dispersive spectroscopy image of Cu/BTiO$_2$-1.6.

TiO_2-containing materials presented revealed exclusive signs indexed to the anatase and rutile TiO_2 crystals at ~25.3° (101) and ~27.3° (110), respectively (Naldoni et al., 2019; Rajaraman et al., 2020). Noticeably, the XRD patterns of the TiO_2-containing materials showed similar intensities at their matched 2θ number, implying that their crystal properties are not substantially altered during their fabrication. Nonetheless, the Cu-related signs did not appear in the XRD spectra of the Cu/$BTiO_2$-1.6, probably owing to the unmeasurable weight of Cu impregnated onto the $BTiO_2$.

The hetero-structural and surface properties of as-constructed Cu/$BTiO_2$-1.6 inspected via TEM and HRTEM are presented in Figs. 2 and 3. Especially, Fig. 2 represents the TEM result and size distribution of Cu/$BTiO_2$-1.6. The TEM image of the material illustrates nanoparticles with diameter range of 10–35, which is comparable to that of P25 TiO_2 diameter (10–30 nm), which are consistent with the results of previous studies Wang et al., 2018 ; Naldoni et al., 2019; She et al., 2020). Besides, the HRTEM mapping figure presents three images of Ti, O, and Cu in Cu/$BTiO_2$-1.6 and their corresponding EDS peaks (Fig. 3), demonstrating the successful incorporation of Cu and $BTiO_2$.

The optical characteristics of pristine TiO_2, $BTiO_2$, Cu/$BTiO_2$, and Cu/$BTiO_2$-1.6 inspected via UV–vis absorption spectroscopy are shown in Fig. 4. The three modified materials ($BTiO_2$, Cu/$BTiO_2$, and Cu/$BTiO_2$-1.6) presented a red-shift in light harvest relative to pristine TiO_2, which results from the elevated visible-light absorption of the former materials. Besides, the visible-light absorption rates of Cu or Cu-incorporated materials (Cu/$BTiO_2$ and Cu/$BTiO_2$-1.6) were greater than that of $BTiO_2$, ascribing to the eminent charge acceptance nature of Cu and Cu, which promotes the carrier separation rates (Liu et al., 2019; Gao et al., 2020; Ge et al., 2020; Li et al., 2020). On the basis of the converted Tauc plots of the UV-vis absorption spectra, the bad edge of pristine TiO_2, $BTiO_2$, Cu/$BTiO_2$, and Cu/$BTiO_2$-1.6 were 3.19, 3.05, 2.87, and 2.91 eV, respectively.

3.2. Photocatalytic CO_2 transformation into CH_4

The photocatalytic CO_2 transformation rates over as-fabricated catalysts were investigated under sunlight exposure. Prior to conducting the main photocatalytic CO_2 transformation experiments, three control experiments were carried out to demonstrate the scientific hypothesis that precious gas CH_4 is solely generated by the photocatalytic transformation of CO_2. Table 1 exhibits the control experiment results for photocatalytic CO_2 transformation into CH_4. First, CH_4 was unobserved in the presence of light but without the addition of a photocatalyst. Second, CH_4 was unobserved in the presence of a photocatalyst but without light. Lastly, CH_4 was yet unobserved in the presence of light and a photocatalyst under CO_2-free conditions. As such, the control experiments demonstrate the abovementioned scientific hypothesis.

The photocatalytic CO_2 transformation rates determined using pristine TiO_2, $BTiO_2$, Cu/$BTiO_2$, and Cu/$BTiO_2$-1.6 are shown in Fig. 5. The pristine TiO_2 and $BTiO_2$ catalysts revealed no significant photocatalytic CO_2 transformation

Table 1. Control experiment results for photocatalytic CO_2 transformation into CH_4*

Irradiation time, h	Control 1	Control 2	Control 3
2	ND	ND	ND
4	ND	ND	ND
6	ND	ND	ND
8	ND	ND	ND
10	ND	ND	ND

*ND represents "not detected"

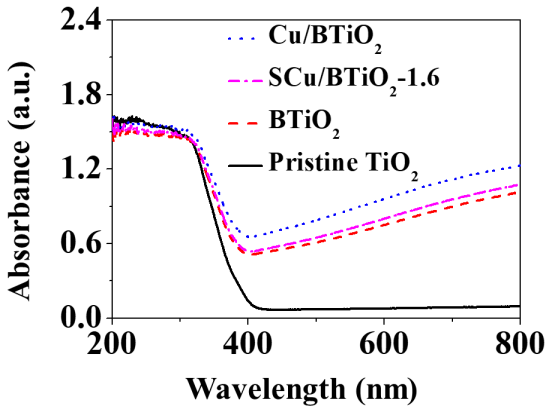

Fig. 4. UV-visible absorption spectra of pristine TiO_2, $BTiO_2$, $Cu/BTiO_2$, and $Cu/BTiO_2$-1.6.

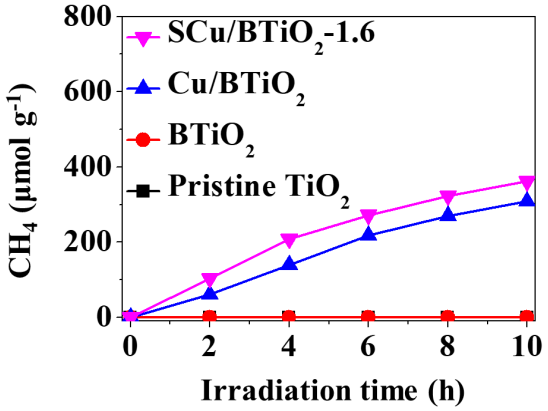

Fig. 5. Time-series CH_4 transformation rates obtained from pristine TiO_2, $BTiO_2$, $Cu/BTiO_2$, and $Cu/BTiO_2$-1.6.

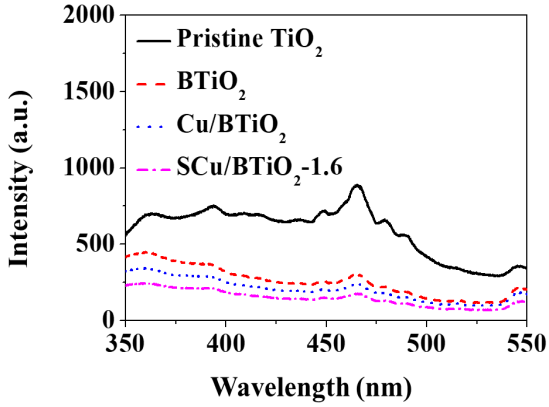

Fig. 6. Photoluminescence emission spectra obtained from pristine TiO_2, $BTiO_2$, $Cu/BTiO_2$, and $Cu/BTiO_2$-1.6.

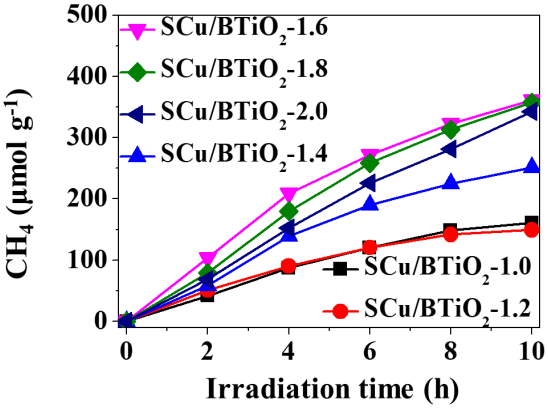

Fig. 7. Time-series CH_4 transformation rates obtained from $Cu/BTiO_2$-1, $Cu/BTiO_2$-1.2, $Cu/BTiO_2$-1.4, $Cu/BTiO_2$-1.6, $Cu/BTiO_2$-1.8, and $Cu/BTiO_2$-2.

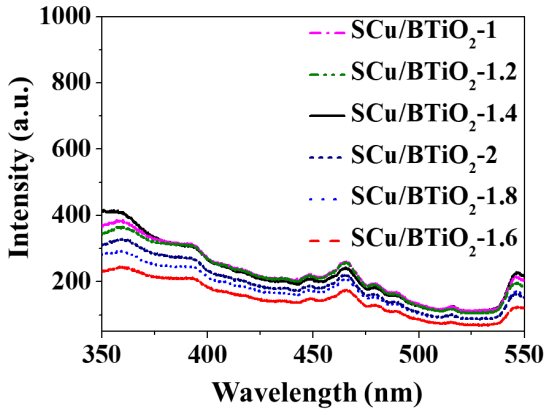

Fig. 8. Photoluminescence emission spectra obtained from $Cu/BTiO_2$-1, $Cu/BTiO_2$-1.2, $Cu/BTiO_2$-1.4, $Cu/BTiO_2$-1.6, $Cu/BTiO_2$-1.8, and $Cu/BTiO_2$-2.

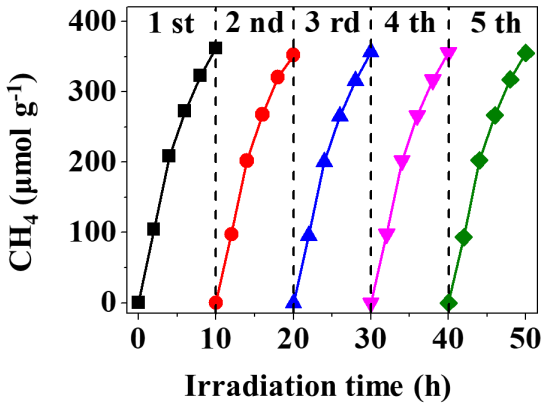

Fig. 9. Recycling test of CH_4 transformation obtained from $Cu/BTiO_2$-1.6.

abilities. Contrarily, Cu/$BTiO_2$ and Cu/$BTiO_2$-1.6 displayed noticeable photocatalytic CO_2 transformation abilities: The photocatalytic CO_2 transformation rates of Cu/$BTiO_2$ were 61, 139, 217, 270, and 309 ㎛ol/g at the irradiation times of 2, 4, 6, 8, and 10 h, respectively; the photocatalytic CO_2 transformation rates of Cu/$BTiO_2$-1.6 were 104, 209, 272, 322, and 361 ㎛ol/g at the irradiation times of 2, 4, 6, 8, and 10 h, respectively. The greatest photocatalytic CO_2 transformation ability of Cu/$BTiO_2$-1.6 is assigned to the excellent electron–hole separation tendency. This statement is demonstrated by Fig. 6, which shows the smaller PL emission signal for Cu/$BTiO_2$-1.6 relative to those of three reference catalysts (pristine TiO_2, $BTiO_2$, and Cu/$BTiO_2$) since a small PL signal indicates a great electron–hole separation tendency (Xie et al., 2020; Xiong et al., 2020).

To ensure that the composition ratio of Cu incorporated into $BTiO_2$ in the Cu/$BTiO_2$ architectures is crucial in CH_4 generation, the CO_2 transformation activities of Cu/$BTiO_2$ architectures with different Cu loadings. As shown in Fig. 7, the CO_2 transformation activities of Cu/$BTiO_2$ architectures are ordered as follows: Cu/$BTiO_2$-1.6 〉 Cu/$BTiO_2$-1.8 〉 Cu/$BTiO_2$-2.0 〉 Cu/$BTiO_2$-1.4 〉 Cu/$BTiO_2$-1.2 〉 Cu/$BTiO_2$-1.0. This pattern of photocatalysts in CO_2 transformation activities are ascribed to their electron–hole separation tendencies, which is demonstrated by the PL emission signals of the surveyed catalysts (Fig. 8). As such, these results imply the existence of an optimum Cu composition incorporated into $BTiO_2$ in the Cu/$BTiO_2$ architectures.

To verify the durability and stability of the Cu/$BTiO_2$ architectures, the time program of CH_4 generation employing the Cu/$BTiO_2$-1.6 architecture was attained under the same experiment conditions. As shown in Fig. 9, the CH_4 generation ratio is constant under prolonged light irradiation up to 50 h. Since this CO_2 transformation activity was evaluated in a closed reaction device, a just small variation in CO_2 transformation activity was observable. To survey the photostability of the architecture, five experiment cycles were carried out. regarding each experiment cycle, the sample powder was washed and positioned in the experimental system. Fig. 9 represents that the content of CH_4 increases with the irradiation time, and no recognizable reduction in CH_4 generation after the final cycle is observable. Consequently, the as-prepared architecture kept eminent photostability during the prolonged experiment.

4. Conclusions

In view of this paper, the photocatalytic CO_2 transformation capability of Cu/$BTiO_2$ was evaluated to investigate if this photocatalyst proceeds the thermodynamically-and kinetically-satisfactory CO_2 transformation into CH_4. The Cu/$BTiO_2$ and Cu/$BTiO_2$ architectures revealed noticeable photocatalytic CO_2 transformation abilities, whereas the pristine TiO_2 and $BTiO_2$ catalysts displayed no significant photocatalytic CO_2 transformation abilities. Moreover, the Cu/$BTiO_2$ architecture exhibited greater photocatalytic CO_2 transformation ability compared with that of the Cu/$BTiO_2$ architecture, which was ascribed to the promoted electron–hole separation tendency of the former. Another important finding is that the composition ratio of Cu incorporated into $BTiO_2$ in the Cu/$BTiO_2$ architectures is crucial in CH_4 generation. The Cu/$BTiO_2$ architecture also revealed eminent photodurability, which was demonstrated by the consecutive experiment cycle. Consequently, the promoted photocatalytic CO_2 transformation capability of Cu/$BTiO_2$ verifies its utilization as an efficient tool in photocatalytic CO_2 transformation.

REFERENCES

Bermejo-López, A., Pereda-Ayo, B., González-Marcos, J. A., González-Velasco, J. R., 2019, Mechanism of the CO_2 storage and in situ hydrogenation to CH_4. Temperature and adsorbent loading effects over Ru-CaO/Al_2O_3 and Ru-Na_2CO_3/Al_2O_3 catalysts, Appl. Catal. B, 256, 117845.

Chen, W., Wang, Y., Liu, S., Gao, L., Mao, L., Fan, Z., Shangguan, W., Jiang, Z., 2018, Non-noble metal Cu as a cocatalyst on TiO_2 nanorod for highly efficient photocatalytic hydrogen production, Appl. Surf. Sci., 445, 527–534.

Chen, W., Han, B., Tian, C., Liu, X., Liang, S., Deng, H., Lin, Z., 2019, MOFs-derived ultrathin holey Co_3O_4 nanosheets for enhanced visible light CO_2 reduction, Appl. Catal. B, 244, 996–1003.

Chen, X., Li, Q., Li, J., Chen, J., Jia, H., 2020, Modulating charge separation via in situ hydrothermal assembly of low content Bi_2S_3 into UiO-66 for efficient photothermocatalytic CO_2 reduction, Appl. Catal. B, 270, 118915.

Cheng, M., Gao, B., Zheng, X., Wu, W., Kong, W., Yan, P., Wang, Z., An, B., Zhang, Y., Li, Q., Xu, Q., 2024, CO_2-assisted rapid synthesis of porphyrin-based Bi-MOFs for photocatalytic CO_2 reduction: An Efficient strategy for carbon cycle, Appl. Catal. B, 353, 124097.

Choi, M., Ahn, C. Y., Lee, H., Kim, J. K., Oh, S. H., Hwang, W., Yang, S., Kim, J., Kim, O. H., Choi, I., 2019, Bi-modified Pt supported on carbon black as electro-oxidation catalyst for 300 W formic acid fuel cell stack, Appl. Catal. B, 253, 187–195.

Dong, H., Meng, X. B., Zhang, X., Tang, H. L., Liu, J. W., Wang, J. H., Wei, J. Z., Zhang, F. M., Bai, L. L., Sun, X. J., 2020, Boosting visible-light hydrogen evolution of covalent-organic frameworks by introducing Ni-based noble metal-free co-catalyst, Chem. Eng. J., 379, 122342.

Fang, Y., Wang, X., 2018, Photocatalytic CO_2 conversion by polymeric carbon nitrides, Chem. Commun., 54, 5674–5687.

Gao, C., Low, J., Long, R., Kong, T., Zhu, J., Xiong, Y., 2020, Heterogeneous single-atom photocatalysts: Fundamentals and applications, Chem. Rev., 120, 12175–12216.

Ge, H., Zhang, B., Liang, H., Zhang, M., Fang, K., Chen, Y., Qin, Y., 2020, Photocatalytic conversion of CO_2 into light olefins over TiO_2 nanotube confined Cu clusters with high ratio of Cu^+, Appl. Catal. B, 263, 118133.

Guo, Q., Fu, L., Yan, T., Tian, W., Ma, D., Li, J., Jiang, Y., Wang, X., 2020, Improved photocatalytic activity of porous ZnO nanosheets by thermal deposition graphene-like g-C_3N_4 for CO_2 reduction with H_2O vapor, Appl. Surf. Sci., 509, 144773.

Ishii, T., Anzai, A., Yamamoto, A., Yoshida, H., 2020, Calcium zirconate photocatalyst and silver cocatalyst for reduction of carbon dioxide with water, Appl. Catal. B, 277, 119192.

Jiang, Z., Zhang, X., Yuan, Z., Chen, J., Huang, B., Dionysiou, D. D., Yang, G., 2018, Enhanced photocatalytic CO_2 reduction via the synergistic effect between Ag and activated carbon in TiO_2/AC-Ag ternary architecture, Chem. Eng. J., 348, 592–598.

Lewis, N. S., 2019, A Prospective on energy and environmental science, Energy Enviro. Sci., 12, 16–18.

Li, X., Yu, J., Jaroniec, M., Chen, X., 2019, Cocatalysts for selective photoreduction of CO_2 into solar fuels, Chem. Rev., 119, 3962–4179.

Li, L., Chang, X., Lin, X., Zhao, Z. J., Gong, J., 2020, Theoretical insights into single-atom catalysts, Chem. Soc. Rev., 49, 8156–8178.

Li, J., Huang, B., Guo, Q., Guo, S., Peng, Z., Liu, J., Tian, Q., Yang, Y., Xu, Q., Liu, Z., Liu, B., 2021, Van der Waals heterojunction for selective visible-light-driven photocatalytic CO_2 reduction, Appl. Catal. B, 284, 119733.

Liao, G. F., Gong, Y., Zhang, L., Gao, H. Y., Yang, G. J., Fang, B. Z., 2019, Semiconductor polymeric graphitic carbon nitride photocatalysts: The ''holy grail'' for the photocatalytic hydrogen evolution reaction under visible light, Energy Environ. Sci., 12, 2080–2147.

Liu, C., Nauert, S. L., Alsina, M. A., Wang, D., Grant, A., He, K., Weitz, E., Nolan, M., Graya, K. A., Notestein, J. M., 2019, Role of surface reconstruction on Cu/TiO_2 nanotubes for CO_2 conversion, Appl. Catal. B, 255, 117754.

Maldonado, M. I., López-Martín, A., Colón, G., Peral, J., Martínez-Costa, J. I., Malato, S., 2018, Solar pilot plant scale hydrogen generation by irradiation of Cu/TiO_2 architectures in presence of sacrificial electron donors, Appl, Catal. B, 229, 15–23.

Majumdar, S. S., Moses-DeBusk, M., Deka, D. J., Kidder, M. K., Thomas, C. R., Pihl, J. A., 2024, Impact of Mg on Pd-based methane oxidation catalysts for lean-burn natural gas emissions control, Appl. Catal. B, 341, 123253.

Naldoni, A., Altomare, M., Zoppellaro, G., Liu, N., Kment, Š., Zbořil, R., Schmuki, P., 2019,

Photocatalysis with reduced TiO_2: From black TiO_2 to cocatalyst-free hydrogen production, ACS Catal., 9, 345–364.

Pan, F., Li, B., Deng, W., Du, Z., Gang, Y., Wang, G., Li, Y., 2019, Promoting electrocatalytic CO_2 reduction on nitrogen-doped carbon with sulfur addition, Appl. Catal. B, 252, 240–249.

Rajaraman, T. S., Parikh, S. P., Gandhi, V. G., 2020, Black TiO_2: A Review of its properties and conflicting trends, Chem. Eng. J., 389, 123918.

She, P., Rao, H., Guan, B., Qin, J. S., Yu, J., 2020, Spatially separated bifunctional cocatalysts decorated on hollow-structured TiO_2 for enhanced photocatalytic hydrogen generation, ACS Appl. Mater. Interfaces, 12, 23356–23362.

Shen, R., Jiang, C., Xiang, Q., Xie, J., Li, X., 2019, Surface and interface engineering of hierarchical photocatalysts, Appl. Surf. Sci., 471, 43–87.

Shi, Q., Li, Z., Chen, L., Zhang, X., Han, W., Xie, M., Yang, J., Jing, L., 2019, Synthesis of SPR Au/$BiVO_4$ quantum dot/rutile-TiO_2 nanorod array architectures as efficient visible-light photocatalysts to convert CO_2 and mechanism insight, Appl. Catal. B, 244, 641–649.

Tang, Y., L, Y., Bao, W., Yan, W., Zhang, J., Huang, Y., Li, H., Wang, Z., Liu, M., Yu, F., 2023, Enhanced dry reforming of CO_2 and CH_4 on photothermal catalyst Ru/ $SrTiO_3$, Appl. Catal. B, 338, 123054.

Ullattil, S. G., Narendranath, S. B., Pillai, S. C., Periyat, P., 2018, Black TiO_2 nanomaterials: A Review of recent advances, Chem. Eng. J., 343, 708–736,

Wang, L., Duan, S., Jin, P., She, H., Huang, J., Lei, Z., Zhang, T., Wang, Q., 2018, Anchored Cu(II) tetra(4-carboxylphenyl)porphyrin to P25 (TiO_2) for efficient photocatalytic ability in CO_2 reduction, Appl. Catal. B, 239, 599–608.

Wang, S. L., Xu, M., Peng, T. Y., Zhang, C. X., Li, T., Hussain, I., Wang, J. Y., Tan, B. E., 2019a, Porous hypercrosslinked polymer-TiO_2-graphene architecture photocatalysts for visible-light-driven CO_2 conversion, Nat. Commun., 10, 676–686.

Wang, R., Shen, J., Sun, K., Tang, H., Liu, Q., 2019b, Enhancement in photocatalytic activity of CO_2 reduction to CH_4 by 0D/2D Au/TiO_2 plasmon heterojunction, Appl. Surf. Sci., 493, 1142–1149.

Wang, Y., Huang, H., Zhang, Z. Wang, C., Yang, Y., Li, Q., Xu, D., 2021, Lead-free perovskite $Cs_2AgBiBr_6$@g-C_3N_4 Z-scheme system for improving CH_4 production in photocatalytic CO_2 reduction, Appl. Catal. B, 282, 119570.

Wei, T., Zhu, Y., Wu, Y., An, X., Liu, L. M., 2019, Effect of single-atom cocatalysts on the activity of faceted TiO_2 photocatalysts, Langmuir, 35, 391–397.

Wu, J., Feng, Y., Li, D., Han, X., Liu, J., 2019, Efficient photocatalytic CO_2 reduction by PeO linked g-C_3N_4/TiO_2-nanotubes Z-scheme architectures, Energy, 178, 168–175.

Xie, C., Niu, Z., Kim, D., Li, M., Yang, P., 2020, Surface and interface control in nanoparticle catalysis, Chem. Rev., 120, 1184–1249.

Xiong, Z., Xu, Z., Li, Y., Dong, L., Wang, J., Zhao, J., Chen, X., Zhao, Y., Zhao, H., Zhang, J., 2020, Incorporating highly dispersed and stable Cu^+ into TiO_2 lattice for enhanced photocatalytic CO_2 reduction with water, Appl. Surf. Sci., 507, 145095.

Xu, S., Chansai, S., Shao, Y., Xu, S., Wang, Y. C., Haigh, S., Mu, Y., Jiao, Y., Stere, C. E., Chen, H., Fan, X., Hardacre, C., 2020, Mechanistic study of non-thermal plasma assisted CO_2 hydrogenation over Ru supported on MgAl layered double hydroxide, Appl. Catal. B, 268, 118752.

Yi, J., Li, H., Gong, Y., She, X., Song, Y., Xu, Y., Deng, J., Yuan, S., Xu, H., Li, H., 2019, Phase and interlayer effect of transition metal dichalcogenide cocatalyst toward photocatalytic hydrogen evolution: The case of $MoSe_2$, Appl. Catal. B, 243, 330–336.

Zeng, C., Zeng, Q., Dai, C., Zhang, L., Hu, Y., 2021, Synergistic effect of surface coated and bulk doped carbon on enhancing photocatalytic CO_2 reduction for $MgIn_2S_4$ microflowers, Appl. Surf. Sci., 542, 148686.

Zhang, H., Li, Y., Wang, J., Wu, N., Sheng, H., Chen, C., Zhao, J., 2021, An Unprecedent hydride transfer pathway for selective photocatalytic reduction of CO_2 to formic acid on TiO_2, Appl. Catal. B, 284, 11692.

Zhao, X., Guan, J., Li, J., Li, X., Wang, H., Huo, P., Yan, Y., 2021, CeO_2/3D g-C_3N_4 heterojunction deposited with Pt cocatalyst for enhanced photocatalytic CO_2 reduction, Appl. Surf. Sci., 537, 147891.

Zhou, M., Wang, S., Yang, P., Huang, C., Wang, X., 2018, Boron carbon nitride semiconductors decorated with CdS nanoparticles for photocatalytic reduction of CO_2, ACS Catal. 8, 4928–4936.

- Research Professor. Dong Jin Kim
  School of Architecture, Civil, Environmental and Energy Engineering, Kyungpook National University
  eastcamp@knu.ac.kr
- Representative Director . Hyun-Cheol Lee
  JIGU Environment and Consulting Inc.
  enviland@naver.com
- Research Director. Seung-Ho Shin
  JIGU Environment and Consulting Inc.
  ssho37@naver.com
- Professor Emeritus. Wan-Kuen Jo
  School of Architecture, Civil, Environmental and Energy Engineering, Kyungpook National University
  wkjo@knu.ac.kr